Enhanced Control and Reproducibility of Nonneutral Plasmas

M. Ahmadi,[1] B.X.R. Alves,[2] C. J. Baker,[3] W. Bertsche,[4,5] A. Capra,[6] C. Carruth,[7] C.L. Cesar,[8] M. Charlton,[3] S. Cohen,[9] R. Collister,[6] S. Eriksson,[3] A. Evans,[10] N. Evetts,[11] J. Fajans,[7] T. Friesen,[2] M.C. Fujiwara,[6] D.R. Gill,[6] J.S. Hangst,[2] W.N. Hardy,[11] M.E. Hayden,[12] C.A. Isaac,[3] M.A. Johnson,[4] S.A. Jones,[2,3] S. Jonsell,[13] L. Kurchaninov,[6] N. Madsen,[3] M. Mathers,[14] D. Maxwell,[3] J.T.K. McKenna,[6] S. Menary,[14] T. Momose,[15] J.J. Munich,[12] K. Olchanski,[6] A. Olin,[6,16] P. Pusa,[1] C.Ø. Rasmussen,[2] F. Robicheaux,[17] R.L. Sacramento,[8] M. Sameed,[3,4] E. Sarid,[18] D.M. Silveira,[8] C. So,[6,10] G. Stutter,[2] T.D. Tharp,[19] J.E. Thompson,[14] R.I. Thompson,[6,10] D.P. van der Werf,[3,20] and J.S. Wurtele[7]

(ALPHA Collaboration)

[1] *Department of Physics, University of Liverpool, Liverpool L69 7ZE, United Kingdom.*
[2] *Department of Physics and Astronomy, Aarhus University, DK-8000 Aarhus C, Denmark.*
[3] *Department of Physics, College of Science, Swansea University, Swansea SA2 8PP, United Kingdom.*
[4] *School of Physics and Astronomy, University of Manchester, Manchester M13 9PL, UK.*
[5] *Cockcroft Institute, Sci-Tech Daresbury, Warrington WA4 4AD, United Kingdom.*
[6] *TRIUMF, 4004 Wesbrook Mall, Vancouver, BC V6T 2A3, Canada.*
[7] *Department of Physics, University of California at Berkeley, Berkeley, CA 94720-7300, USA.*
[8] *Instituto de Física, Universidade Federal do Rio de Janeiro, Rio de Janeiro 21941-972, Brazil.*
[9] *Department of Physics, Ben-Gurion University of the Negev, Beer-Sheva 84105, Israel.*
[10] *Department of Physics and Astronomy, University of Calgary, Calgary, AB T2N 1N4, Canada.*
[11] *Department of Physics and Astronomy, The University of British Columbia, Vancouver, BC V6T 1Z1, Canada.*
[12] *Department of Physics, Simon Fraser University, Burnaby, BC V5A 1S6, Canada.*
[13] *Department of Physics, Stockholm University, SE-10691, Stockholm, Sweden.*
[14] *Department of Physics and Astronomy, York University, Toronto, ON M3J 1P3, Canada.*
[15] *Department of Chemistry, The University of British Columbia, Vancouver, BC V6T 1Z1, Canada.*
[16] *Department of Physics and Astronomy, University of Victoria, Victoria, BC V8P 5C2, Canada.*
[17] *Department of Physics and Astronomy, Purdue University, West Lafayette, Indiana 47907, USA.*
[18] *Soreq NRC, Yavne, 81800, Israel.*
[19] *Physics Department, Marquette University, P.O. Box 1881,Milwaukee, WI 53201-1881, USA.*
[20] *IRFU, CEA/Saclay, F-91191, Gif-sur-Yvette Cedex, France.*

(Dated: November 30, 2017)

The simultaneous control of the density and particle number of nonneutral plasmas confined in Penning-Malmberg traps is demonstrated. Control is achieved by setting the plasma's density by applying a rotating electric field while simultaneously fixing its axial potential via evaporative cooling. This novel method is particularly useful for stabilizing positron plasmas, as the procedures used to collect positrons from radioactive sources typically yield plasmas with variable densities and particle numbers; it also simplifies optimization studies that require plasma parameter scans. The reproducibility achieved by applying this technique to the positron and electron plasmas used by the ALPHA antihydrogen experiment at CERN, combined with other developments, contributed to a ten-fold increase in the antiatom trapping rate.

We report experiments that employ a novel plasma physics technique to achieve a dramatic improvement in the control and reproducibility of nonneutral plasmas. This development was implemented in the ALPHA antihydrogen experiment at CERN, where it facilitated optimization of the myriad procedures involved in trapping antihydrogen and contributed to a ten-fold increase in the trapping rate [1]. This increase in the trapping rate was critical to the success of observations of the 1S–2S transition [2] and hyperfine splitting [3] in antihydrogen. The new technique is potentially applicable to a variety of nonneutral plasma systems and regimes, including those used in particle accelerator studies [4], ion mass spectrometry [5], fluid dynamics [6, 7], positron beam creation [8–10], atomic clocks [11], and positron-electron pair plasmas [12].

Nonneutral plasmas contain particles with the same charge polarity, and are often confined as ellipsoids in Penning-Malmberg traps (see Fig. 1). Such traps use a strong axial magnetic field $\mathbf{B}$ for radial confinement and an electrostatic well for axial confinement; the latter is formed by biasing a series of electrically isolated, hollow cylinders arrayed along the magnetic axis.

The zero-temperature equilibrium of a plasma held in a Penning-Malmberg trap is a rigid rotor of constant density n [13]. The plasma rotates at frequency f due to the local $\mathbf{E}\times\mathbf{B}$ drift velocity; here, the electric field $\mathbf{E}$ comes from the charge of the plasma. At non-zero plasma temperatures T [14], this equilibrium is modified such that the fluid rotation rate (set by the $\mathbf{E}\times\mathbf{B}$ drift combined with the diamagnetic drift) is constant across the plasma.

Antihydrogen is synthesized in the ALPHA apparatus

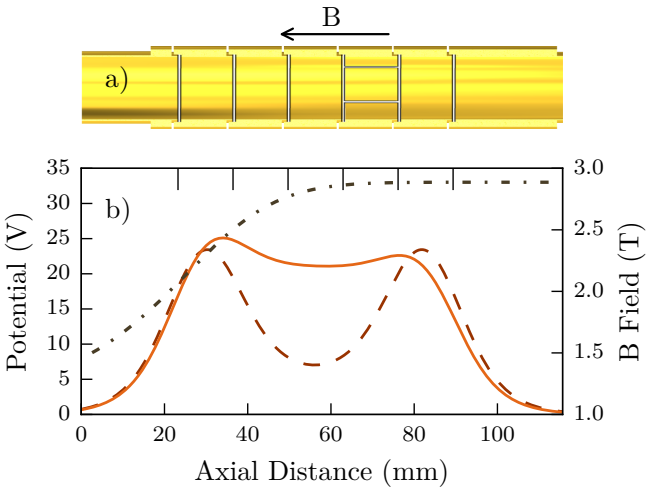

FIG. 1. a) Partial schematic of one of ALPHA's Penning-Malmberg traps, showing the axial magnetic field **B**, seven of the electrically-isolated cylindrical electrodes, and one rotating wall electrode (fifth in from the left) with six isolated azimuthal sectors; the inner radius of the electrodes is 14.8 mm. b) Typical initial (dashed) and final (solid) electrostatic potentials used in the stabilization procedure, and the axial magnetic field (dot-dash).

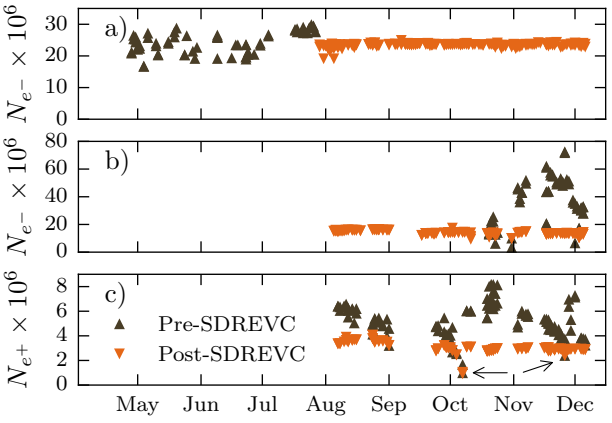

FIG. 2. Pre- (▲) and post- (▼) SDREVC measurements: a) plasma electron number N_{e-} in the catching trap; b) plasma electron number N_{e-} in the atom trap; and c) plasma positron number N_{e+} in the atom trap. SDREVC was implemented at the end of July 2016, so only pre-SDREVC data are shown prior to that date. Beginning in August, the pre-SDREVC numbers in a) are off scale. The arrows in c) indicate instances where the positron moderator efficiency decreased and the number of pre-SDREVC positrons dropped below the desired post-SDREVC value; the number was recovered by regrowing the moderator.

by mixing positron and antiproton plasmas in a shallow magnetic minimum neutral atom trap, and traps antiatoms colder than 0.54 K [15, 16]. ALPHA uses two Penning-Malmberg traps, the antiproton catching and antihydrogen mixing traps, to prepare and mix plasmas; descriptions are given in Ref. [15]. Due to the extreme sensitivity of the antiatom trapping rate on the parameters of the plasmas, much experimental effort has been devoted to their optimization. Historically, the trapping rate suffered from short term and long term variations in plasma densities and particle numbers. The positron plasma parameters varied by up to a factor of two, likely due to changes in the solid-neon positron moderator and the buffer gas in the positron accumulator [17]. Smaller variations in the electron plasmas were likely due to drifts in the thermionic electron source compounded by the large magnetic field gradient between the source and the trap. These variations led us to use an autoresonant mixing technique [18, 19] which, while relatively insensitive to small changes in plasma parameters, was suboptimal for trapping; our plasma manipulations required frequent tuning.

The technique described here controls two of the most critical plasma parameters, the number of plasma particles N and the density n. Rotating wall electric fields [20] in the strong drive regime (SDR) [21] are applied simultaneously with evaporative cooling (EVC) [22] electrostatic well potentials. Hence, the process is called SDREVC. After introducing SDREVC, the electron and positron plasmas became highly reproducible so long as the pre-SDREVC N was at least marginally higher than the desired post-SDREVC N.

Figure 2 shows the dramatic stabilization of electron and positron plasmas obtained with SDREVC. The electron plasmas in Fig. 2a were held in a uniform 3 T axial field. The electron plasmas in Fig. 2b were held in a uniform 1 T axial field while the positron plasmas in Fig. 2c were held in a 3 T axial field with a slight gradient as shown in Fig. 1b. The standard deviation of the number of particles in Fig. 2a diminished from 14% without SDREVC to less than 3% with SDREVC; even larger improvements are observed in the data in Figs. 2b and 2c. Below we show a simple theory that motivated this procedure, the techniques we use to achieve it, and the range over which the theory models our experimental results.

We assume throughout that $k_B T \ll e\phi$, where ϕ is the potential difference over the radius of the plasma due to its own charge and e is the elementary charge. This is equivalent to assuming that the plasma is at least several Debye lengths in radius, and is often taken as a requirement that a cloud of charged particles is a plasma. In the zero-temperature limit, the $\mathbf{E}\times\mathbf{B}$ rotation frequency f of the plasma is

$$f = \left(\frac{e}{4\pi\epsilon_0 B}\right) n, \qquad (1)$$

where ϵ_0 is the permittivity of free space. Experimentally, we impose a rotation frequency f, and hence fix n.

The on-axis self potential ϕ_c of an infinitely-long, zero-temperature plasma is

$$\phi_c = \frac{ner_p^2}{4\epsilon_0}\left[1 + 2\ln\left(\frac{R_w}{r_p}\right)\right], \tag{2}$$

where R_w and r_p are the electrode and plasma radii respectively, and the electrode walls are assumed to be at ground. If the plasma is confined in a relatively shallow electrostatic well with depth equal to ϕ_c, and if n is controlled by f, then Eq. (2) admits only one solution for r_p. Furthermore, the total number of plasma particles is given by

$$N = \int^V n\, dV = n\pi r_p^2 L, \tag{3}$$

where the plasma length L is assumed to be long enough that axial end effects can be neglected. Thus, using SDREVC to simultaneously control the rotation frequency f and the on-axis potential ϕ_c fully specifies all the plasma parameters in the zero-temperature limit; this is the essence of the SDREVC technique.

The density of a nonneutral plasma in a Penning trap can be manipulated by applying rotating electric fields at frequencies near the plasma's natural rotation frequency. The fields are created by applying appropriately phased oscillating potentials to the azimuthally-sectored rotating wall electrodes (see Fig. 1). This technique, called rotating wall compression, was pioneered by Huang *et al.* [23], and has been used extensively in the nonneutral plasma community.

As first noted by Danielson and Surko [24], the plasma rotation frequency f can lock to the rotating wall drive frequency in the strong drive regime. Since the density, in turn, is governed by the plasma rotation frequency, this allows control of the density by varying the drive frequency. In ALPHA, a plasma a few centimeters long can be in the strong drive regime when one end of the plasma is dri[ven at frequencies varying between 50 kHz and 1 MHz with sinusoidal potentials in the range of 1 to 5 V. It is notable that strong drive operation can be achieved even in the presence of spatial variations in the magnetic field (see Fig. 1) [25].

The on-axis potential ϕ_c is controlled via evaporative cooling, a procedure which has been used in ALPHA to cool both antiprotons [22] and positrons. Evaporative cooling is performed by lowering the axial potential barriers confining a nonneutral plasma such that the most energetic particles escape; typically, the barriers are lowered asymmetrically so that particles escape from only one end of the plasma. Examples of initial and final potentials are shown in Fig. 1b. As with any evaporative procedure, the remaining trapped particles are cooler than those in the initial plasma. In the zero-temperature limit, this will set the potential of the plasma to ϕ_c.

Evaporative cooling and rotating wall compression have competing effects; the rotating wall heats the plasma while the evaporative cooling cools the plasma, and the rotating wall radially compresses the plasma while evaporative cooling radially expands the plasma [22]. To overcome these competing side effects, it is necessary to experiment with different potential well shape manipulations, axial plasma positions relative to the rotating wall electrode, and rotating wall amplitudes and frequencies. Once tuned, SDREVC is robust, and adjusting the tuning parameters can yield an optimized post-SDREVC plasma. The plasma's radial profile is diagnosed by extracting the plasma onto a micro-channel plate (MCP) attached to a phosphor screen and imaging the fluorescence with a CCD camera [26]. The plasma radius, normalized net intensity, and line-integrated density are determined from the resultant MCP images by applying a generalized Gaussian fit to the plasma profile,

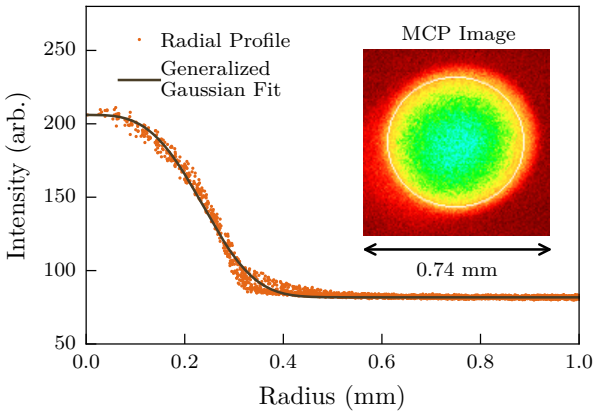

FIG. 3. Image data (orange circles) and generalized Gaussian fit (brown line) of the intensity as a function of radius corresponding to the inset MCP image of an electron plasma.

$$f(r) = ae^{-\left(\frac{r}{b}\right)^n} + c \tag{4}$$

where a is the overall scaled line density, b is the radius of the plasma after scaling to account for the lower magnetic field at the MCP location relative to the initial plasma location, $n \approx 2$ scales the fall-off region, and c accounts for the image background. The density can then be found numerically [27]. The plasma particle numbers can be measured directly with the Faraday cup, or they can be determined from the MCP image by calibrating the normalized net intensity, of the MCP images to absolute numbers; calibration factors are determined separately by sequentially depositing identical plasmas onto the MCP and the Faraday cup. Typical radii, numbers of particles, and densities of the plasmas after SDREVC were on the order of 0.5 mm, 10^7, and $10^8\,\mathrm{cm}^{-3}$ respectively. An example MCP image with its generalized Gaussian fit of a post-SDREVC plasma is shown in Fig. 3.

Figures 4 and 5 show the results of experiments de-

signed to test SDREVC. Due to the long duty cycle for making positron plasmas and an additional desire to better control the large electron plasmas used for cooling antiprotons, we opted to use electron plasmas to test and characterize SDREVC. We prepared electron plasmas with a range of pre-SDREVC particle numbers by varying the electron loading procedures, and a range of pre-SDREVC densities by driving the plasmas with different rotating wall frequencies. In Fig. 4 the potential well during SDREVC was ramped from the initial to final states similar to those shown in Fig. 1b over 20 s, while 2.5 V rotating wall potentials at 450 kHz were continually applied. Later tests showed that reducing the SDREVC time to 10 s produced similar results. The post-SDREVC plasmas are highly reproducible; Figs. 4a and b confirm that the number of particles and plasma density post-SDREVC are invariant over a large range of initial particle numbers. Fig. 4c confirms a similar invariance in the post-SDREVC density for a large range of initial densities. Notably, SDREVC can increase or decrease the density. For comparison, the measurements of plasmas after EVC only in Fig. 4 are not independent of the initial conditions.

In Fig. 4, each data point represents the average of 20 measurements; the standard error of the mean of each point is smaller than the size of the markers, so error bars were omitted. The shot-to-shot variation of the particle number and density after SDREVC was about 1%, which is the precision limit of our diagnostics. However, long term drifts in post-SDREVC plasma parameters, as apparent in Fig. 2, can be larger than 1%. These drifts are thought to be due to slow variations in other experimental parameters such as the decay of the persistent current in the solenoid producing the axial magnetic field and its periodic resets.

Figure 5 shows that by varying the tuning parameters, SDREVC can produce plasmas with a wide range of particle numbers and densities. In Fig. 5a, an order of magnitude range in the number of particles post-SDREVC was achieved by varying the final depth of the potential well while driving the plasma with a 2.5 V, 700 kHz rotating wall. From Eq. (2), it is easy to show that at constant density, ϕ_c should scale with N, given normalization points ϕ_{c_0}, r_{p_0}, and N_0, as

$$\phi_c = \phi_{c_0}\left(\frac{N}{N_0}\right)\frac{1+\ln\left(\frac{R_w^2}{r_{p_0}^2}\frac{N_0}{N}\right)}{1+\ln\left(\frac{R_w^2}{r_{p_0}^2}\right)}. \qquad (5)$$

The solution to this equation is plotted in Fig. 5a, normalized around the measured values $N_0 = 3.1\times10^7$ and $r_{p_0} = 0.42$ mm found at $\phi_{c_0} = 8$ V. The nonlinear corrections from the logarithmic terms in Eq. (5) are small.

Figures 5b and 5c show the effect of changing the rotating wall frequency f. As expected, in Fig. 5b the density n increases linearly with f while in the strong drive regime. The dependence of the radius r_p on f comes from the solution to the differential equation

$$\frac{\mathrm{d}r_p}{\mathrm{d}f} = -\frac{r_p}{2f}\left[1+\frac{1}{2\ln(R_w/r_p)}\right], \qquad (6)$$

but is only marginally different from the solution ignoring the logarithmic correction, $r_p = r_{p_0}\sqrt{f_0/f}$. In Fig. 5b, the solution for r_p is normalized around $r_{p_0} = 0.33$ mm and $f_0 = 450$ kHz.

Figure 5c plots the final number N as a function of f, which can be calculated from Eqs. (1), (3), and (6). We observe that SDREVC can control the plasma's density or its number of particles by an order of magnitude, while additional data (not shown) has extended the ranges to even higher numbers of particles and lower densities post-SDREVC. The excellent agreement of the data and the theoretical predictions in Figs. 5b and 5c up to 750 kHz

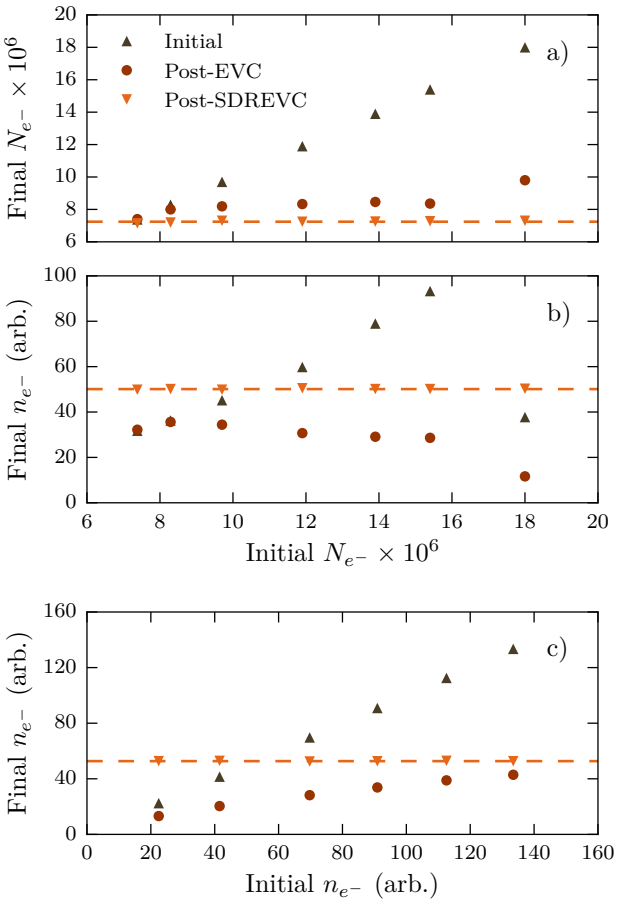

FIG. 4. Initial (▲), post-EVC (●), and post-SDREVC (▼) measurements for a variety of plasma parameters. a) The final number of electrons as a function of the initial number of electrons; b) the final plasma density as a function of the initial number of electrons; and c) the final density as a function of the initial density. The density refers to the results of an axially-integrated MCP diagnostic and has arbitrary units. The orange lines mark the average post-SDREVC values.

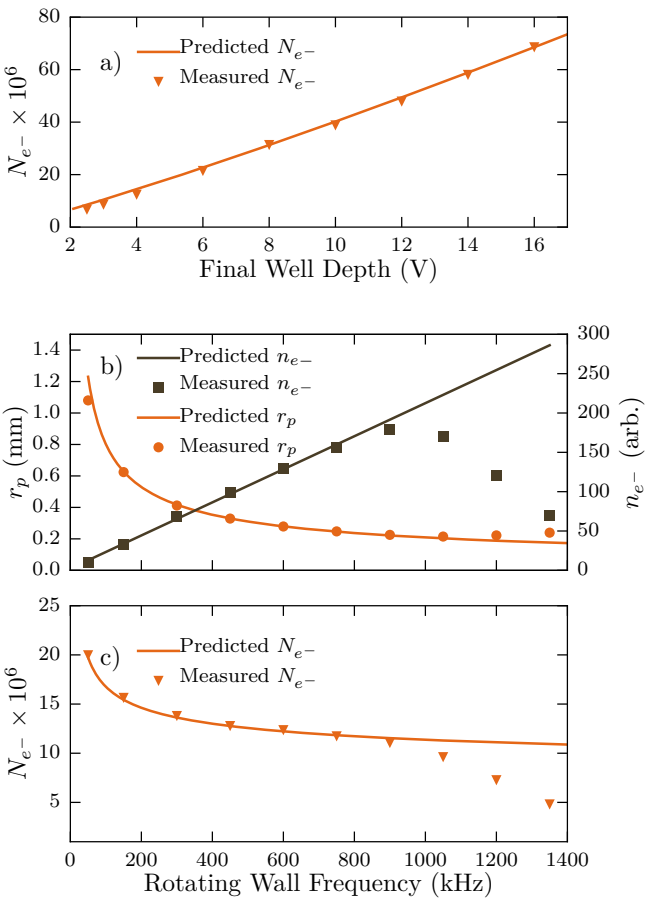

FIG. 5. Measured numbers (▼), densities (■), and radii (●); predicted values, normalized at 450 kHz, are indicated by the lines. a) Number of electrons retained in different well depths when driven with a 700 kHz rotating wall; b) plasma radius and plasma density; and c) number of electrons retained in a 4V potential well as a function of the rotating wall frequency.

provide strong evidence that the plasma is in the strong drive regime at lower frequencies; above this frequency, it departs from this regime. The standard deviation of the data in Fig. 5 was again smaller than the markers, so error bars have been similarly omitted. Two of the 400 measurements taken for Figs. 4b and 4c were excluded because the plasma compression failed for unknown reasons.

The scalings developed from Eqs. (1) and (2) are formally valid only for zero-temperature plasmas. Measurements show that the plasma temperatures can be as high as 300 K during the SDREVC process. At these finite temperatures at least two of the zero-temperature assumptions are no longer valid. First, Eq. (2) assumes that the plasma is a rigid rotor of uniform density; at non-zero temperatures, the plasma's radial profile falls off over a few Debye lengths. Computational analysis of the equilibrium equations developed by Prasad and O'Neil [14] shows that, in the experimentally relevant regime (potential well depths greater than 2 V, and rotation frequencies below 1.5 MHz), variations in the calculated post-SDREVC central density for temperatures of 30–300 K are less than 1%. Second, evaporative cooling relies on the axial escape of the highest energy particles in the plasma distribution; the actual plasma potential ϕ_c is several $k_B T$ less than the confining EVC potential. This can cause changes in N of 5–10% over the operating range. Note, however, that the temperature profile is roughly similar over multiple shots; thus, these effects do not necessarily impact the reproducibility of plasmas treated with SDREVC.

Other data (not shown) demonstrate that single or repeated cycles of sequential, rather than simultaneous, SDR and EVC, are not as efficacious. Such sequential SDR and EVC cycles were used, but not reported [28], in Refs. [8] and [9].

In summary, simultaneously applying a rotating wall and evaporative cooling can reproducibly stabilize cold, nonneutral plasmas. By changing the depth of the potential well or the frequency of the applied rotating electric field, the plasma density and total particle number can be tailored over a large range of values. This technique was employed to stabilize plasmas against fluctuations in their initial conditions. This stabilization has been particularly dramatic for positron plasmas and was a significant contributor to recent factor-of-ten improvements in antihydrogen trapping rates and can be applied to many other nonneutral plasma systems.

We thank Dr. Matthias Reinsch for his help developing the finite temperature theory. This work was supported by: the European Research Council through its Advanced Grant programme (JSH); CNPq, FAPERJ, RENAFAE (Brazil); NSERC, NRC/TRIUMF, EHPDS/EHDRS (Canada); FNU (NICE Centre), Carlsberg Foundation (Denmark); ISF (Israel); STFC, EPSRC, the Royal Society and the Leverhulme Trust (UK); DOE, NSF (USA); and VR (Sweden).

[1] M. Ahmadi *et al.* (ALPHA Collaboration), Nature Comm. **8**, 681 (2017).
[2] M. Ahmadi *et al.* (ALPHA Collaboration), Nature **541**, 506 (2017).
[3] M. Ahmadi *et al.* (ALPHA Collaboration), Nature **548**, 66 (2017).
[4] E. P. Gilson, R. C. Davidson, P. C. Efthimion, R. Majeski, E. A. Startsev, H. Wang, S. Koppell, and M. Talley, Phys. Plasmas **20**, 055706 (2013).
[5] A. G. Marshall, Int. J. Mass Spect. **200**, 331 (2000).
[6] C. F. Driscoll and K. S. Fine, Phys. Fluids B **2**, 1359 (1990).
[7] A. J. Peurrung, J. Notte, and J. Fajans, J. Fluid Mech. **252**, 713 (1993).
[8] T. R. Weber, J. R. Danielson, and C. M. Surko, Phys. Plasmas **15**, 012106 (2008).
[9] T. R. Weber, J. R. Danielson, and C. M. Surko, Phys. Plasmas **17**, 123507 (2010).
[10] M. R. Natisin, J. R. Danielson, and C. M. Surko, Phys. Plasmas **23**, 023505 (2016).
[11] J. J. Bollinger, D. J. Wineland, and D. H. E. Dubin, Phys. Plasmas **1**, 1403 (1994).
[12] H. Saitoh, T. S. Pedersen, U. Hergenhahn, E. V. Stenson, N. Paschkowski, and C. Hugenschmidt, Journal of Physics: Conference Series **505**, 012045 (2014).
[13] R. C. Davidson, *Physics of Nonneutral Plasmas* (Addison-Wesley, Redwood City, 1990).
[14] S. A. Prasad and T. M. O'Neil, Phys. Fluids **22**, 278 (1979).
[15] C. Amole *et al.* (ALPHA Collaboration), Nucl. Instr. Meth. Phys. Res. A **735**, 319 (2014).
[16] G. B. Andresen *et al.* (ALPHA Collaboration), Nature Phys. **7**, 558 (2011).
[17] T. J. Murphy and C. M. Surko, Phys. Rev. A **46**, 5696 (1992).
[18] G. B. Andresen *et al.* (ALPHA Collaboration), Nature **468**, 673 (2010).
[19] G. B. Andresen *et al.* (ALPHA Collaboration), Phys. Rev. Lett. **106**, 025002 (2011).
[20] R. G. Greaves and C. M. Surko, Phys. Rev. Lett. **85**, 1883 (2000).
[21] J. R. Danielson and C. M. Surko, Phys. Rev. Lett. **94**, 035001 (2005).
[22] G. B. Andresen *et al.* (ALPHA Collaboration), Phys. Rev. Lett. **105**, 013003 (2010).
[23] X.-P. Huang, F. Anderegg, E. M. Hollmann, C. F. Driscoll, and T. M. O'Neil, Phys. Rev. Lett. **78**, 875 (1997).
[24] J. R. Danielson and C. M. Surko, Phys. Plasmas **13**, 055706 (2006).
[25] J. Fajans, Phys. Plasmas **10**, 1209 (2003).
[26] G. B. Andresen *et al.* (ALPHA Collaboration), Rev. Sci. Instrum. **80**, 123701 (2009).
[27] C. So, *Antiproton and positron dynamics in antihydrogen production*, Ph.D. thesis, University of California, Berkeley (2014).
[28] James Danielson (private communication).